An electrokinetically-controlled immunoassay for simultaneous detection of multiple microbial antigens

Yali Gao[1], Guoqing Hu[1], Frank Y. H. Lin[2], Philip M. Sherman[2] and Dongqing Li[1]

[1]Department of Mechanical and Industrial Engineering, University of Toronto, 5 King's College Road, Toronto, Ontario, M5S 3G8, Canada

[2]Departments of Paediatrics and Laboratory Medicine & Pathobiology, University of Toronto, Toronto, Ontario, Canada

Abstract

An electrokinetically-controlled heterogeneous immunoassay microchip for multiple analyte detection was developed in this study. Numerical simulation was employed to study the transport processes in a microfluidic network (μFN). The operation parameters obtained from numerical simulation were then applied to immunoassay experiments. The effectiveness of automatic electrokinetic control was demonstrated in a separate experiment using fluorescein dye for flow visualization. The immunoassay microchip was made of poly(dimethylsiloxane)(PDMS)/PDMS-coated glass using soft lithography and replica molding. Multi-antigen immobilization was accomplished by adsorbing the antigen molecules onto a PDMS-coated glass slide and by using a μFN. Immobilized lysate antigen of *Escherichia coli* O157: H7 at different concentrations was assayed and the lower detect limit was 3 μg/mL. The assay also displayed very good specificity, when different microbial lysate antigens were immobilized, including *Escherichia coli* O157: H7 and *Helicobacter pylori*, and the primary and secondary antibody solution contained a mixture of different species of antibodies. The time required for the immunoassay, from antigen coating to signal detection, was only one hour. While still an un-optimized prototype, this automatic-operating, high-throughput immunoassay microchip shows a great potential in detecting multiple pathogenic infections efficiently for clinical applications.

Key words: immunoassay; electrokinetic; numerical simulation; microfluidic; *Escherichia coli* O157:H7.

1. Introduction

Immunoassay is based on the specific antibody-antigen reaction, which is highly selective and sensitive. Since its introduction in the 1960s, immunoassay has become one of the most important analytical methods and has been widely applied to a variety of fields, such as biochemical, environmental, agricultural and forensic studies, as well as medical diagnoses (Diamandis and Christopoulos, 1996).

With the booming development of lab-on-a-chip technique or micro-total analysis system (μ-TAS) since the 1980s, miniaturization of the immunoassay technique has become an area of interest. First, the integration of homogeneous immunoassays onto microchips was reported (Chiem and Harrison, 1997; Wang et al, 2001), which was based on capillary electrophoresis separation. Then, microchip-based heterogeneous immunoassays, which involve a solid phase for the immobilization of one of the reactants, were also investigated in some research works (Rossier and Girault, 2001; Sato et al, 2001; Eteshola and Leckband, 2001; Sia et al, 2004; Lin et al, 2004, A). These works demonstrated significantly improved reaction kinetics of the heterogeneous immunoassay compared with conventional techniques, due to the reduction in diffusion distance and increase in surface-to-volume ratio. The time for the immunoassay could be reduced from hours and days to within an hour (Rossier and Girault, 2001; Sato et al, 2001). Also, the reagent consumption could be reduced to several or tens of microliters, while more than

100 μL is required in the 96-well microtiter plate, a conventional device for carrying out immunoassay. It has also been shown in these works that the miniaturized immunoassay can reach a level of sensitivity comparable to that of the conventional technique.

Currently, there is still a large gap between the studies on miniaturized heterogeneous immunoassay and clinical application. Of the many obstacles, two major ones are - lack of automation and low throughput. Automation of immunoassay is very important because immunoassay is a multi-step analysis that involves many operation processes, such as sequential solution loading and washing. Conducting these operations manually is not only very inefficient, but also easy to introduce human error and thus reduce the reliability of the assay. In conventional immunoassays, automation can be achieved using robotic techniques (Chan, 1996). How to automate the immunoassay operation on a lab-on-a-chip device, is a major challenge. As for the throughput, devices for conventional immunoassay, such as the 96-well microtiter plates, allow for simultaneous handling of many samples. The throughput of the lab-on-a-chip-based immunoassay needs to be improved in this aspect. Some relevant studies have been reported in recent years. A miniaturized micromosaic immunoassay (μMIA) was proposed (Bernard et al., 2001; Wolf et al, 2004), which is based on patterning different molecules (antibody or antigen) onto parallel regions on a surface by means of a microfluidic network (μFN)(Delamarche et al, 1997; Delamarche et al, 1998). This enabled localized immunoreaction between the antigen and antibody so that a multi-analyte immunoassay can be realized. In another study, a similar multi-sample screening immunosensor was developed and tested with several clinical fluids (Rowe et al., 1999). The function of serial dilution can also be integrated onto such an immunoassay chip (Jiang et al., 2003).

However, little work has been done on automation of the heterogeneous immunoassay lab-on-a-chip. This is due to the fact that most of the aforementioned studies were based on pressure-driven flow to realize the multi-step solution operations, e.g. solution loading and washing. The pressure difference was created by either capillary force or syringe pumping and aspiration. Automation of such systems will inevitably require the complicated robotic technique and external tubing, valves and other mechanical devices.

On the other hand, automation of microfluidic processes can be more easily achieved with electrokinetically-driven (EK-driven) flow, which has been extensively used for solution pumping and dispensing in microfluidic devices (Whitesides and Stroock, 2001; Li, 2004; Stone et al, 2004). In EK-driven flow, the liquid motion in a microchannel is driven by an applied electric field, so that flow switching and solution replacing can be realized by simply changing the applied electric field and thus no moving part is required.

There have been only very few studies on the EK-driven heterogeneous immunoassay lab-on-a-chip. In the first reported study in this area (Dodge et al., 2001), protein A was immobilized on the channel surface and its affinity for Immunoglobulin G (IgG) was tested using EK-driven competitive immunoassay. However, the μFN used was complex and the flow was not well confined to the designed paths. In a later study (Linder et al., 2002), EK-driven flow was employed to conduct a competitive immunoassay for human IgG on a biopassivated symmetric cross microchannel. In their two-step immunoassay, antibody dispensing, incubation and washing were realized by applying three different electric fields manually.

It is easy to understand that the difficulty in controlling the multi-step microfluidic processes increases dramatically with the complexity of the μFN. For a complicated immunoassay involving more than one immunoreactions, the number of required microchannel branches and wells (holding different solutions) increases, and hence the number of electrodes. In such a case, it would be very difficult to find the appropriate values

of the controlling parameters for each step, i.e. the electric potentials at different wells, merely through experiments. One good solution to this problem is to use Computational Fluid Dynamics (CFD) to simulate the microfluidic processes and to determine these parameters. CFD is a powerful tool to build virtual prototypes and to simulate the performance of proposed designs in many engineering fields, including the microfluidic area (Ermakov et al, 1998; Erickson and Li, 2003). Although liquid flow in the microchannel can be obtained by solving for the electric field alone (Cummings et al, 2000; Qiu and Harrison, 2001; Ajdari, 2004), CFD was employed in this study because it can provide complete information on both the flow and time-dependent mass transport processes.

In this work, numerical simulations and experimental studies were combined together for the first time to study an electrokinetically-controlled heterogeneous immunoassay. Operation parameters acquired from the numerical simulations, i.e. the electric potentials and the duration of the steps, were applied to experimental studies. Automatic sequential solution operations, i.e., reagent loading, washing and flow switching, were facilitated by a programmable high-voltage sequencer. The effectiveness of using numerical simulation to realize the electrokinetically-controlled processes in an immunoassay was demonstrated.

In addition, we increased the throughput by testing a multi-analyte immunoassay on the same chip. A μFN bearing a pattern of parallel straight channels was used to carry out multiple antigen immobilization. It was shown that by depositing a thin film of PDMS on a glass slide, the antigen immobilization could be realized by simply using passive adsorption, i.e. “coating”. Two different microbial pathogens, *Escherichia coli* O157:H7 and *Helicobacter pylori*, were studied as models. *E. coli* O157:H7 is recognized as a major cause of hemorrhagic colitis and can induce other life-threatening diseases (Tarr and Neill, 2001). *H. pylori* affects half of the world’s population and can cause gastritis, peptic ulcer disease (Sherman et al, 1999) and gastric cancers (Uemura et al, 2001). The immunoassay in this study is a two-step indirect heterogeneous immunoassay, with fluorescent (TRITC)-labelled secondary antibody for signal generation.

2.Chip design, physical model and numerical computation

2.1 Chip design

The immunoassay microchip is shown in Fig. 1. Figure 1 (a) provides a schematic illustration of the H-shaped μFN and Fig. 1(b) is a picture of the microchip. The overall dimension of the μFN is 23 $\times$ 10 mm^2. In designing the μFN, we have considered:

(1) The μFN should include at least one well and one supply channel for each reagent. In addition, there should be one well for the waste, to avoid cross-contamination. Therefore, for the immunoassay in this study, four wells would be required, each for the primary antibody, secondary antibody, washing buffer or waste solution, as indicated in Fig. 1(a).

(2) The channels should be as short as possible to minimize transport distance, but long enough to avoid the cross-contamination between the different reagents due to possible small fluctuations in flow driving force.

(3) The overall size of the μFN should fit onto a 75$\times$25 mm^2 microscope glass slide commonly used in labs.

(4) While the reagent consumption is kept reasonable, the size of wells should be made as large as possible to minimize the change of liquid levels in the wells that could cause undesired flows driven by hydrostatic pressure difference.

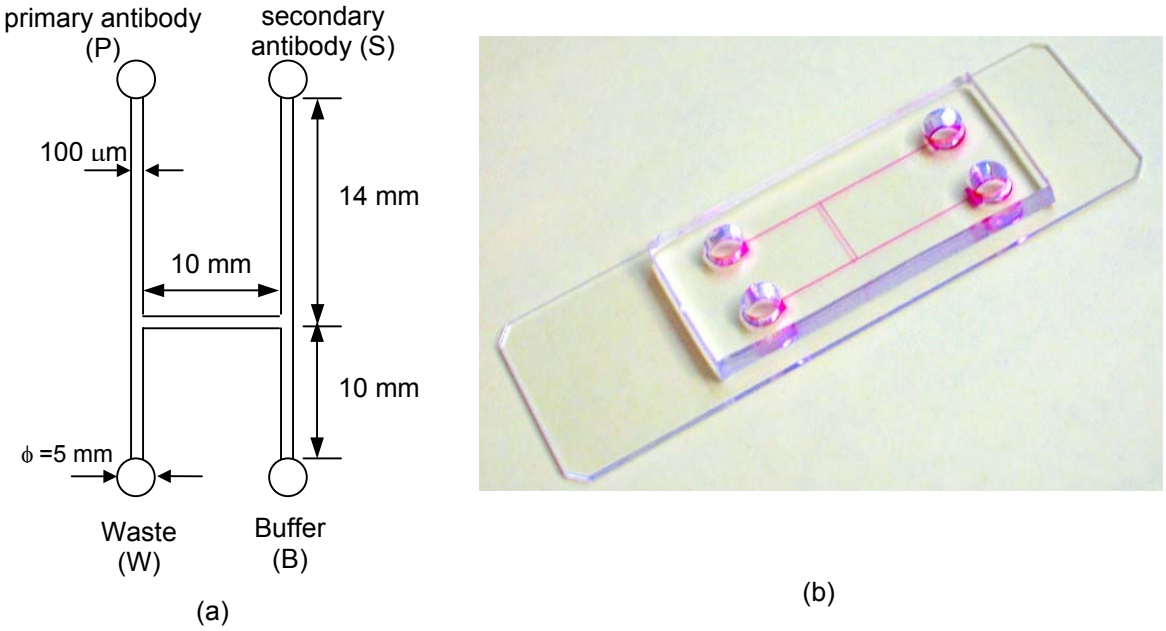

Figure 1: (a) A schematic illustration the μFN used in the immunoassay microchip (not proportional to actual size). All the channels are 100 μm wide and 20 μm high. Overall dimension of the chip is 23 mm x 10 mm. The diameter of all the wells is 5 mm. (b) A picture of the immunoassay microchip (The channel is filled with rhodamine B to illustrate the geometry).

(5) From the reaction kinetics point of view, the cross section of the microchannels should be large to transport more reagents. However a larger cross section will increase the effects of the undesirable pressure-driven flow. Moreover, it can also lead to significant Joule heating. After some preliminary testing using 8 μm-, 20 μm- and 40 μm-high channels, 20 μm-high microchannels were chosen in this study.

2.2 physical model

The driving force in electrokinetically-driven flow is the electric body force existing in the near-wall electric double layer (EDL) (Hunter, 1981; Masliyah, 1994) where the net charge density is not zero. Electroosmosis arises when the liquid solution moves relative to the solid wall under an applied electric field. Under ideal conditions (uniform surface and bulk solution properties, thin EDL, etc.), the electroosmotic velocity can be calculated as $\vec{V}_{eo} = \mu_{eo}\vec{E}$ (Cummings et al, 2000), where μ_{eo} is the electroosmotic mobility and can be expressed as $\mu_{eo} = -\varepsilon_0 \varepsilon \zeta / \eta$. Here ε is the dielectric constant of the liquid, ε_0 is the permittivity in vacuum, ζ is the zeta potential on the channel wall and η is the dynamic viscosity of liquid. The motion of the charged particles under an applied electric field is called electrophoresis. Also, $\vec{V}_{ep} = \mu_{ep}\vec{E}$, where μ_{ep} is the electrophoretic mobility and can be expressed in a similar way as μ_{eo}, with ζ being the zeta potential on the particle. The movement of the protein molecules in the microchannel is a superposition of electroosmosis in the bulk flow and electrophoresis of themselves. The mobilities μ_{eo} and μ_{ep} were measured through experiments, as will be described in the next section.

Steady electroosmotic flow (EOF) and transient sample transportation were considered in modeling. The steady-state simplification can be justified because EOF reaches steady state instantaneously (in approximately several milliseconds) once an electric field is applied along the channels (Patankar and Hu, 1998). Another simplification was to decrease the dimensionality of the problem from 3-D to 2-D because all the

channels had a constant depth and the surface properties of the channels were assumed uniform.

The governing equations for the transport processes in the μFN include:

- The Laplace equation for the electric field:

$$\nabla^2\Phi = 0 \qquad (1)$$

where Φ is the applied electric potential;

- Steady-state incompressible Navier-Stokes equations,

$$\vec{V}_{eo}\cdot\nabla\vec{V}_{eo} = -\frac{1}{\rho_f}\nabla P + \nu\nabla^2\vec{V}_{eo} + \frac{\rho_e}{\rho_f}\vec{E} \qquad (2)$$

$$\nabla\cdot\vec{V}_{eo} = 0 \qquad (3)$$

where $\vec{V}_{eo}$ is the bulk electroosmotic flow field, *P* is the pressure, *v* is the kinematic viscosity of the fluid and ρ_f is the density of the fluid. The driving force, i.e. the electric body force, exists only within the near-wall EDL whose thickness is less than 10 nm in our case. Therefore, the electric body force term $\rho_e\vec{E}$ could be neglected from Equation (2), with slip boundary conditions at the solid walls being introduced instead. That is, $\vec{V}_{slip} = \mu_{eo}\vec{E}$ at solid walls.

- Transient mass transport equation,

$$\frac{\partial C_i}{\partial t} + (\vec{V}_{eo} + \vec{V}_{ep})\cdot\nabla C_i = D_i\nabla^2 C_i \qquad (4)$$

where C_i is the concentration of the *i*-th sample (e.g. primary antibody, secondary antibody), $\vec{V}_{eo} + \vec{V}_{ep}$ is the net velocity of the protein molecules, D_i is the diffusion coefficient of the *i*-th sample.

Boundary conditions for Eq.s (1)-(4) are given as following,

at inlets, $\Phi = \Phi_i$, $\frac{\partial\vec{V}_{eo}}{\partial n} = 0$, $P = 0$, $C_i = C_{i0}$;

at outlets, $\Phi = \Phi_i$, $\frac{\partial\vec{V}_{eo}}{\partial n} = 0$, $P = 0$, $\frac{\partial C_i}{\partial n} = 0$;

at walls, $\frac{\partial\Phi}{\partial n} = 0$, $\vec{V}_{eo} = \vec{V}_{slip} = \mu_{eo}\vec{E}$, $\frac{\partial P}{\partial n} = 0$, $\frac{\partial C_i}{\partial n} = 0$.

where Φ_i is the electric potential applied to each well. In the computation of the sample concentration field, the concentration distribution obtained from the previous operation will be used as the initial condition of the next operation.

2.3 Numerical computation

The numerical computation has been described in detail in a previous work (Hu et al, in press). In brief, augmented Lagrangian method (Bertsekas, 1982) was adopted to solve the Navier-stokes Equations. The transient advection-diffusion concentration equation (4) was discretized using the implicit Euler backward scheme. Finite element method was employed to numerically solve the Eq.s (1)-(4) and the computational domain was divided into a set of unstructured 6-node triangular finite elements. The discretized systems of

algebraic equations were solved using an incomplete LU factorization preconditioned Bi-CGSTAB solver (van der Vorst, 1992).

2.4 Determination of the operating parameters

In practice, each step in the immunoassay, e.g. reagent dispensing and washing, requires a corresponding electric field. In numerical simulation, the applied electric potentials at the wells were adjusted following a trail-and-error optimization process until the designed mass transportation process was obtained and no undesired reagent leakage occurred. Once the applied electric field for a certain step was determined, the duration of the step could be decided from the simulation of the time-dependent concentration field. Theoretically, a dispensing/washing process is complete when the reactant is delivered into/out of the reaction region.

3. Experimental

3.1 Microchannel fabrication

The substrate was prepared by coating a thin film of PDMS (Polydimethylsiloxane) on a glass slide to utilize the hydrophobicity of PDMS for protein immobilization. However, due to its low thermal conductivity, the PDMS layer cannot be too thick. Otherwise, significant Joule heating can occur (Jones and Grushka, 1989) and the resulting high temperature may not only affect the flow but also impair the immunoreaction. Spin-coating was employed to create the thin film. Briefly, PDMS polymer base and curing agent were mixed at a ratio of 15:1 (w/w). One milliliter of the mixture was deposited onto a 75×25 mm^2 acetone-cleaned glass slide and degassed for one hour at –34 kPa (gauge). After that, the glass slide with liquid PDMS on it was placed in a spin-coater to create a PDMS layer of about 10 μm. The PDMS layer was then cured at 75℃ for two hours.

Two different μFNs were used. One was straight channels in parallel (40 μm high) used for antigen immobilization, as shown in Fig. 3 (a). The straight channels were extended at the ends to give convenience to making wells. The other μFN was H-shaped microchannels (20 μm high) used for conducting the immunoassay, as shown in Fig. 1. The channel width was 100 μm for both μFNs. For the straight-channel μFN, the gap between the channels was 80-100 μm. The channels were made from PDMS through replica molding and the masters used were fabricated by soft lithography technique (Xia and Whitesides, 1998). The fabrication protocol was as described elsewhere (Biddiss et al, 2004). Briefly, the masters were prepared by first spin-coating a 20 μm- or 40 μm–thick film of SU-8 25 negative photoresist onto a glass slide. After pre-baking, a photomask bearing a certain microchannel geometry, i.e. a parallel straight channel μFN or an H-shaped μFN, was placed on top of the film. The photoresist film covered with the mask was then exposed to UV light. After post-baking and developing, the master could be obtained. Then a 15:1 (w/w) mixture of PDMS polymer base and curing agent was poured over the master. After degassed for one hour, the mixture was cured at 75℃ for three hours.

The PDMS replica bearing a certain channel pattern was then cut and peeled from the master. A hole was bored at each end of the channel to form a well. The internal diameters of the holes were 3 mm and 5 mm for the straight channel μFN and H-shaped μFN, respectively.

3.2 Antigen preparations and reagents

The procedures for preparing bacterial antigens were reported previously (Lin et al, 2004 A, B). Briefly, *H. pylori* strain ATCC 49503 was cultured on 5% sheep blood agar plates and incubated at 37 ℃ under microaerophilic conditions for 72 hours. Bacteria were

then inoculated into Brucella broth with 10% fetal bovine serum and grown overnight with gentle shaking. *Escherichia coli* O157:H7, strain CL-56 was cultured on 5% sheep blood agar plates at 37 ℃ overnight, and stored at 4 ℃ after that. Bacteria were then cultured in static, nonaerated Penassay broth overnight at 37 ℃. *Lactobacillus rhamnosus*, strain R011, used as a negative control, was cultured on 5% sheep blood agar plates at 37℃ overnight, and then inoculated into De Mann Ragosa Sharpe broth overnight. The liquid cultures were then centrifuged and the supernatants removed. Bacterial pellets were re-suspended in phosphate-buffered-saline (PBS) and washed for 4 times. The pellets were re-suspended in RIPA buffer (10 mM Tris HCl, pH 8.0, 150 mM NaCl, 0.5% Trition X-100) containing a mixture of proteinase inhibitors cocktail (Roche Molecular Biochemicals, Mannheim, Germany) for 40 min and lysates were centrifuged and the supernatants collected as whole bacterial proteins. After being assayed for protein concentration, these lysate antigens were diluted to the final concentrations using a coating buffer (consisting of 0.03M $NaHCO_3$ and 0.02M Na_2CO_3, pH 9.6).

The washing buffer, 25 mM tris-HCl buffer (TBS) with pH 7.5, was made from tris-HCl base (Sigma-Aldrich Canada Ltd., Ontario, Canada) and double distilled water. The blocking buffer was prepared by adding 5% (w/v) bovine serum albumin (BSA) in 25 mM TBS. Polyclonal rabbit anti-*H. pylori* antibody was obtained from DAKO (Glostrup, Denmark). Polyclonal goat anti-*E. coli* antibody was from KPL (Gaithersburg, ML). The two secondary antibodies, TRITC-conjugated donkey anti-rabbit IgG and TRITC-conjugated donkey anti-goat IgG, were both purchased from Jackson ImmunoResearch Laboratories, Inc. (West Grove, PA). The anti-*E. coli* antibody and anti- *H. pylori* antibody were diluted to 1:25 and 1:8 with the blocking buffer solution, respectively, so that their final concentration were both 40 μg/mL. Both secondary antibodies were diluted to 1:25 with the blocking buffer before use, with a final concentration of 60 μg/mL.

3.3. Electrokinetic mobility measurement

The electroosmotic mobility μ_{eo} of the 25 mM TBS solution was measured by using the current-monitoring method (Huang et al, 1988; Sze et al, 2003), with a straight microchannel. To render its surface condition the same as that of the channels used in the immunoassay experiments, the straight microchannel was incubated with antigen and blocked before the mobility measurement. Then, a diluted buffer solution (90% of the original concentration, i.e. 25 mM) was electroosmotically pumped through the channel (with a length of l) at a constant applied voltage $\Delta\Phi$. The current was monitored and allowed to be stable. An undiluted buffer (25 mM) was then electroosmotically driven through the channel to displace the diluted buffer. The time required for the current to reach a new plateau was recorded as t. The electroosmotic mobility could be obtained as,

$$\mu = \frac{V}{E} = \frac{l/t}{\Delta\Phi/l} = \frac{l^2}{\Delta\Phi \cdot t} \qquad (5)$$

To measure the net electrokinetic mobility of the antibodies, a method using the antigen-antibody binding reaction was employed. The mobilities of the two TRITC-conjugated secondary antibodies were measured separately. Briefly, a straight microchannel that had been subject to full-length antigen coating, blocking and primary antibody incubation was used for the experiment. The two wells were filled with the corresponding TRITC-conjugated secondary antibody solution and TBS buffer solution, respectively. TRITC-conjugated secondary antibody was electrokinetically pumped into a part of the channel during a certain time period, t. Then the flow was stopped to allow incubation for three minutes, during which the TRITC-conjugated antibodies would bind with the primary antibodies on the channel wall. At the same time, the channel was observed

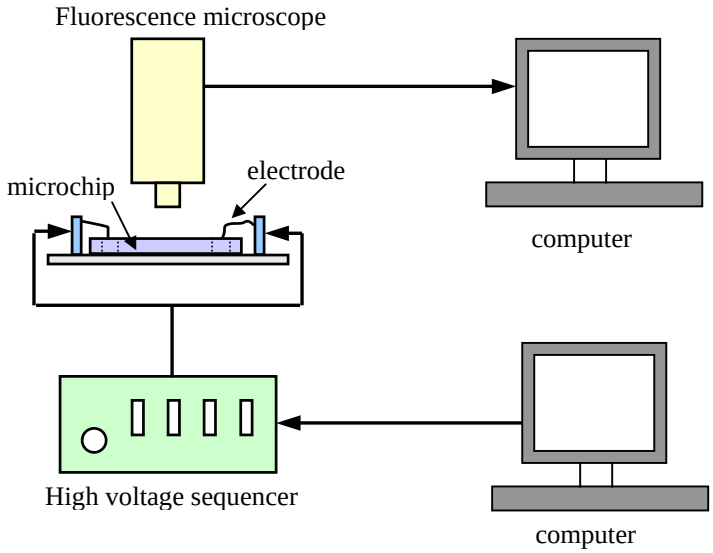

Figure 2: A schematic of the experimental setup and imaging system.

under a fluorescence microscope so that any possible pressure-driven flow could be eliminated by adjusting the levels of the solutions in the two wells. After incubation, buffer solution was electrokinetically delivered through the channel to wash out the excess antibodies. Viewing under the fluorescence microscope, the length of the channel that gave a fluorescence signal was taken as *l*. Then the net electrokinetic mobility of the antibodies in the TBS buffer could be calculated also using Eq. (5).

3.4 Automatic flow control

The power supply used in the electrokinetically-controlled immunoassay experiments is HVS448 High Voltage Sequencer (Labsmith, Livermore, CA). This high voltage sequencer has eight independent outputs, which are programmable through the Sequence software (Labsmith, Livermore, CA).

The experimental setup is shown in Fig. 2. The high voltage sequencer received the programmed sequences from the computer, which defined the output voltages and duration for each step. The output channels of the sequencer were connected with platinum electrodes, which were placed into solutions in the wells of the microchip. The signal detection part will be described later.

An experiment using fluorescein dye to illustrate the mass transportation was conducted in order to test whether the computational-acquired electric field can control the flow as expected and to assess the performance of the high voltage sequencer in automatically switching the output voltage.

The experiment was carried out on a microchip with the H-shaped μFN. The procedures were as follows. A PDMS slab bearing an H-shaped μFN and a clean glass slide were both put into a plasma sterilizer for 30 s to allow for surface oxidation. Immediately after removal from the sterilizer, the PDMS slab and the glass slide were brought into contact with each other and an irreversible sealing was formed. 25 mM sodium carbonate/bicarbonate (SCC) buffer was then added to one of the wells and it would fill the channel spontaneously due to the capillary pressure (Kim et al, 1995).
In the experiment, the two wells designed for the primary and secondary antibodies (P and S in Fig. 1) in the μFN were both filled with 20 μL of 10 μM fluorescein diluted with 25mM SCC. The other two wells were filled with 20 μL of 25 mM SCC buffer. The operation steps were same as those in an immunoassay. After the sequencer was triggered to run,

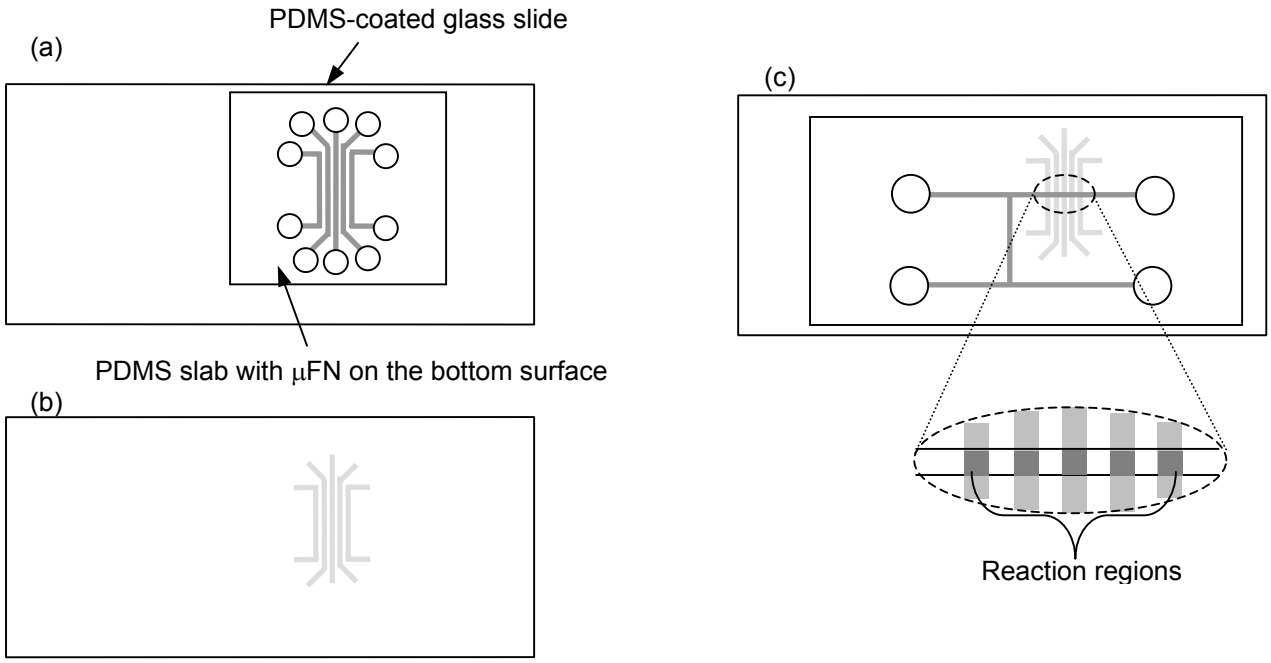

Figure 3: The preparation process of the immunoassay (schematics are not proportional to actual size). (a) antigen immobilization using the parallel straight channel μFN; (b) antigen molecules patterned on the surface after a 15-minute immobilization; (c) H-shaped μFN put across the antigen pattern. The intersections of the parallel regions of antigen coating and the H-shaped μFN became reaction regions in later immunoassay experiments.

the two junctions of the H-shaped μFN were successively viewed under a fluorescence microscope and images were automatically taken at an interval of one second.

3.5 Electrokinetically-driven immunoassay

The first step of the immunoassay was the immobilization of antigens on the substrate. μFNs with parallel channels were used to achieve the multi-antigen immobilization, as shown in Fig. 3 (a). The PDMS slab bearing the μFN was plasma-hydrophilized for 1 minute before it was brought into conformal contact with the PDMS-coated glass slide. Then, 1.5 μL of lysate antigen (1 μg/mL to 30 μg/mL) was added to one well of each channel, after it filled the channel spontaneously, the same amount of the lysate antigen was put into the other wells. The microchip was then covered with a piece of micro cover glass to prevent the solution from evaporation.

After 15 minutes of passive adsorption at room temperature, the micro cover glass was removed and the microchip was put under a deep vacuum for 6 minutes to produce a quick evaporation of the solutions. The position of the μFN was marked from the reverse side of the glass slide and the PDMS slab was peeled from the chip. The chip was then rinsed with 1 mL 25 mM TBS buffer and 3 mL double distilled water, successively. The microchip with patterned antigen is shown in Fig. 3 (b).

Another PDMS slab bearing the H-shaped μFN was put into the plasma sterilizer and hydrophilized for one minute. It was then put into conformal contact with the antigen-patterned substrate, with the left arm of the “H” crossing the antigen pattern orthogonally, as shown in Fig. 3 (c). Special care was taken during this process to keep a constant relative position between H-shaped μFN and the antigen pattern each time. The intersections of the parallel regions of coated antigen and the H-shaped μFN, in shape of an array of squares as shown in the enlargement in Fig. 3 (c), became the reaction regions when antibody molecules were delivered through the H-shaped μFN.

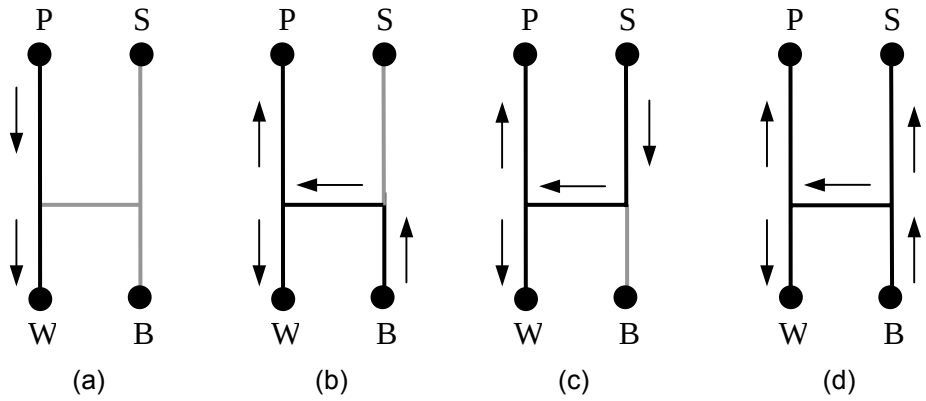

Figure 4: The sequential steps of the immunoassay. Solution delivery occurs in the dark colored channels whereas in the light colored channels, the solution is almost stagnant. The arrows indicate the flow direction. (a) dispensing and incubation of the primary antibody; (b) washing of the primary antibody; (c) dispensing and incubation of the secondary antibody; (d) washing of the secondary antibody.

Once the channel was made, blocking buffer, 5% BSA in 25mM TBS, was delivered into the μFN and incubated for 10 minutes. After blocking, each well was washed and filled with the corresponding solutions as shown in Fig. 1 except that the waste well was filled with TBS buffer solution.

The immunoassay consisted of six steps. The first three were about the primary antibody: (1) dispensing of primary antibody to the reaction region; (2) incubation, for the antibody molecules to diffuse onto the surface and react with the immobilized antigens; (3) washing of the excess primary antibody out of the reaction region. Step (4)-(6) correspond to the same operations for the secondary antibody. The realization of these processes in the H-shaped μFN is illustrated in Fig. 4. The applied electric potentials and duration for each step were set with the Sequence software. After the sequencer started to run, the operations were carried out and switched automatically and no manual operation was required during the assay.

3.6 Detection and image analysis

Fluorescent signals were detected by using a Leica DM-LB fluorescence microscope (Leica Microsystems, Richmond Hill, Canada). A mercury arc lamp was used as the light source. Images were captured using a Retiga 12-bit cooled CCD camera (QImaging corp. BC, Canada) at an exposure time of 5 s unless indicated otherwise. Signals from the assay, an array of squares, were captured in one single fluorescent image.

The intensity of the fluorescence was analyzed by using Openlab 3.1.5 imaging software (Improvision Inc, Lexington, MA). Fluorescent intensities from both the square signal regions and their neighboring background regions were quantified. Then, the signal for each square reaction region was determined as the difference between its own intensity and the average intensity of its two neighboring regions, to eliminate the influence of background fluorescence.

4. Results and discussion

4.1 Measurement of electrokinetic mobility

It was found by the current-monitoring method that the electroosmotic mobility, μ_{eo}, of the 25 mM TBS buffer was 1.7×10^{8} m^2/V·s. The net electrokinetic mobilities, μ_{net}, of both TRITC-conjugated donkey IgGs were found to be also approximately $1.5\sim1.7\times10^{8}$ m^2/V·s. For the protein molecules, the net electrokinetic velocity is given by $\vec{V}_{net} = \vec{V}_{eo} + \vec{V}_{ep}$. Since

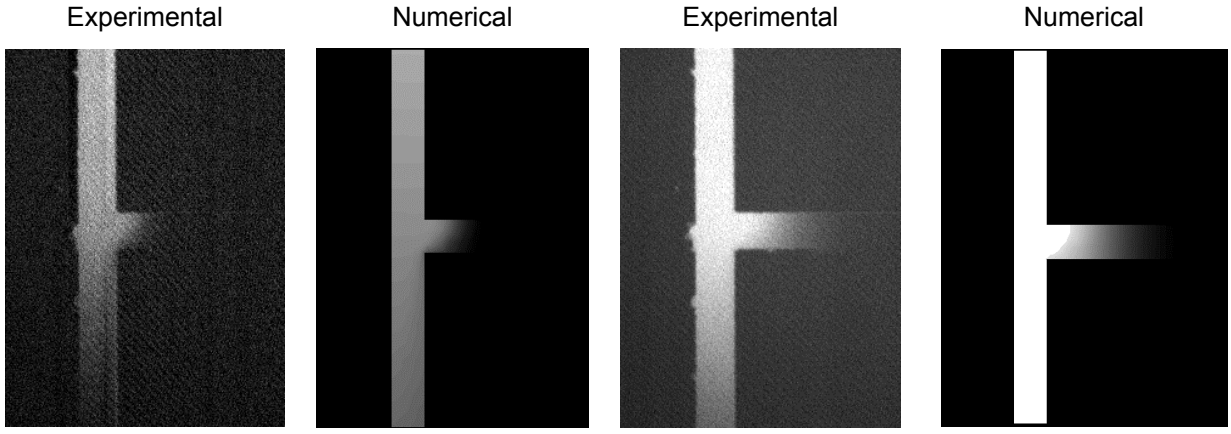

Figure 5 The first solution dispensing process (step 1) – experimentally and numerically acquired concentration fields on the left junction of the "H". t_1 and t_2 indicate the lapse time after step 1 started.

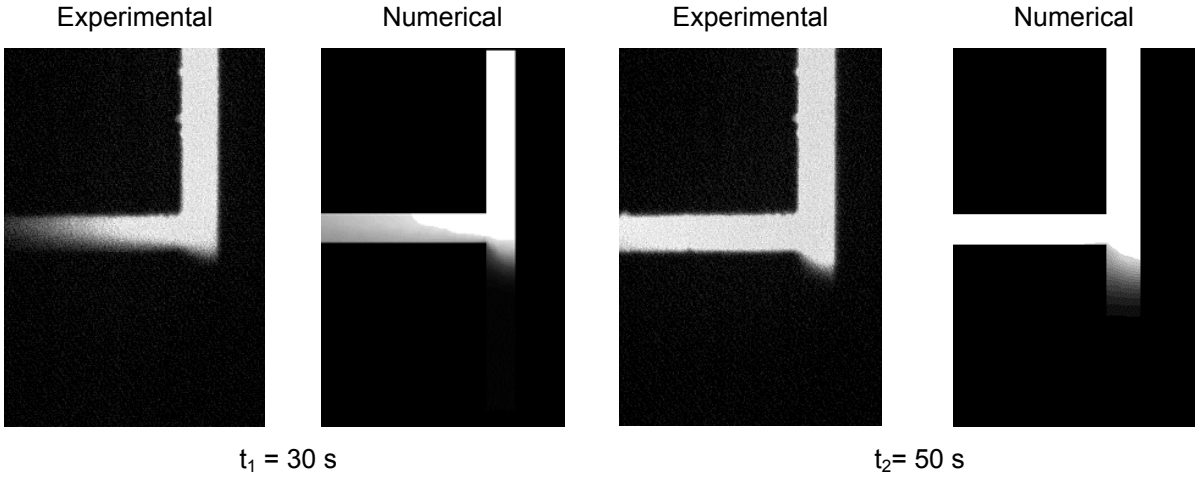

Figure 6: The second solution dispensing process (step 4) – experimentally and numerically acquired concentration fields on the right junction of the "H". t_1 and t_2 indicate the lapse time after step 4 started.

μ_{net} is approximately the same as μ_{eo}, the electrophoresis of the antibody molecules in the 25 mM TBS with pH 7.5 was negligible in this study.

4.2 Test of automatic flow control

The values of the operation parameters were the same as those used in the immunoassay, as shown in Table 1. The electroosmotic mobility of the SCC buffer and the electrophoretic mobility of the fluorescein dye were measured previously as 5.9×10^{8} m^2/V·s and -3.3×10^{8} m^2/V·s, respectively (Biddiss et al, 2004). These lead to a net mobility of the fluorescein dye of 2.6×10^{8} m^2/V·s, about 50% higher than the antibodies. Therefore, the dispensing/washing time would be sufficient.

Figure 5 and Fig. 6 show the images taken at the two junctions. Since the washing steps were easier to control, the images shown were all from the sample dispensing process (step 1 and step 3) to show if the sample transport followed the designed flow path strictly. The two images in each figure were taken at two different moments when sample dispensing at the region was incomplete and complete, respectively. The predicted concentration fields from numerical simulation at the same moment were also provided for comparison.

Table 1: Operation parameters of the immunoassay

Step	operation	Applied potentials at wells (*V*)				Duration (*s*)
		Φ_W	Φ_B	Φ_S	Φ_P	
1	Dispensing primary Ab	0	95	100	250	210
2	Incubation	0	47.5	50	125	300
3	Washing primary Ab	0	500	300	0	120
4	Dispensing secondary Ab	0	265	500	0	350
5	Incubation	0	132.5	250	0	300
6	Washing secondary Ab	0	500	0	0	300

The experimental results displayed a very good agreement with the numerical predictions, on both the time-dependence and the sample concentration field. From Fig. 5, the leakage of the sample into the horizontal arm was very small. The case was the same in Fig. 6, where the sample from the "S" well was precisely delivered into the horizontal arm as designed. Sample diffusion into the branches would occur during the 5-min incubation, but the distance traveled was short, less than 2 mm. Therefore, cross-contamination between reagents will not occur during the assay. However, if the size of the wells were much smaller, e.g. 3 mm, undesirable pressure-driven flows could be more easily induced and the concentration field might be affected.

4.3 Automatic electrokinetically-controlled immunoassay

The operation parameters used in the electrokinetically-controlled immunoassay are given in Table 1. Incubation was carried out under a continuous-flow condition, when the electric field strength was reduced by half compared to the reagent dispensing process. The continuous-flow mode is believed to be superior to the stagnant mode for incubation in two aspects. First, from a reaction kinetics point of view, if the antibody molecules are continuously delivered to the reaction region under the flow condition, the antibody concentration will be supplemented and the antigen-antibody binding reaction will be promoted. Second, the influence of the undesirable pressure-driven flow will be minimized with the existence of a much stronger EOF. Incubation time was set to be 5 minutes for both the primary and the secondary antibody. The total time for the immunoassay was 26 minutes and 20 seconds.

Figure 7 shows the fluorescence image of an immunoassay with the same concentration of coating antigen, 10 μg/mL *E. coli* lysate, on the four different sites. The exposure time in taking the image was reduced to 3 seconds to avoid saturation of the signals. Consistent fluorescence was acquired among the sites, with a variation coefficient of quantified intensities of only 14.5%. This result indicated that the immunoreaction happened almost to the same extent on different sites, since they were closely placed over a region of only 1.2 mm long. Thus, the incubation times and other conditions were comparable. Therefore, they could each be independently analyzed to assess the localized immunoassay.

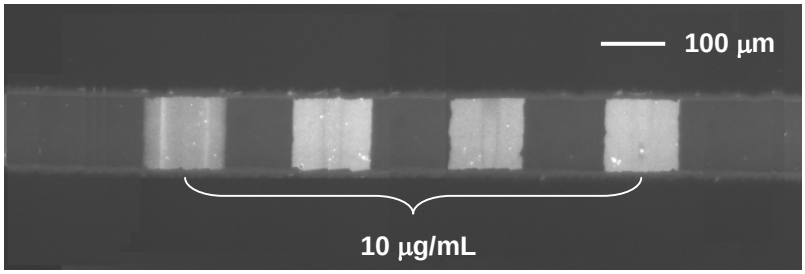

Figure 7: Performance assessment of the multi-target immunoassay. Concentration of coating *E. coli* lysate antigen was 10 μg/mL for all sites.

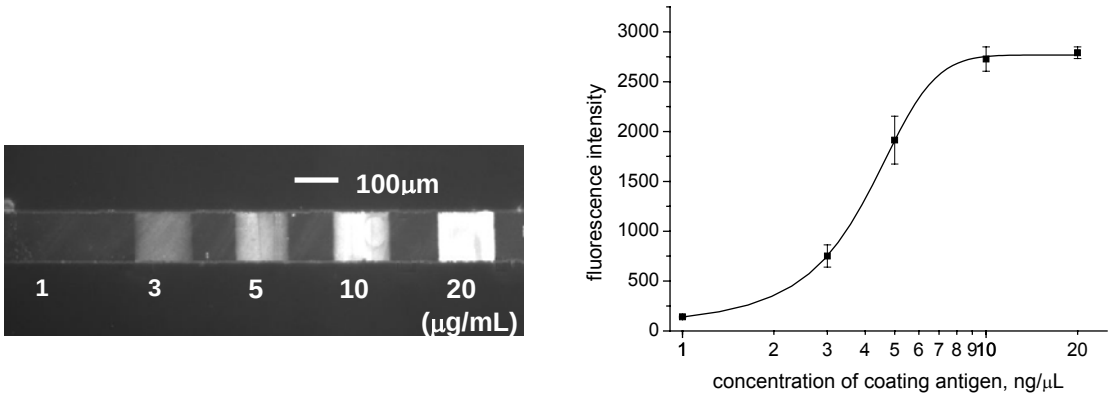

(a) (b)

Figure 8: Fluorescent signal dependence on the concentration of the coating antigen. (a) fluorescent image of the immunoassay. Concentrations of coating *E. coli* lysate antigen were (μg/mL, from left to right): 1, 3, 5, 10, 20. (b) The quantified intensity-concentration dependence.

In order to investigate the dependence of the signals on the concentration of coating antigen, different dilutions of *E. coli* lysate antigen, from 1 μg/mL to 20 μg/mL, were applied to the five coating channels. Figure 8 (a) shows the fluorescence image acquired after the immunoassay. Figure 8 (b) is the plot of the quantified results, where the data points are fitted using a sigmoidal function. As shown, *E. coli* antigens were reliably detected in the concentration range between 3 μg/mL and 20 μg/mL. But the signal showed saturation as the concentration of coating antigen approached 10 μg/mL. The detection limit of 3 μg/mL is comparable to the 4 μg/mL obtained in a previous study, using a hand-held immunosensor as well as the conventional dot-blot immunoassay (Lin et al, 2004, B). Usually, to study the dependence on coating concentration of the immunoassay, several experiments under different coating concentrations have to be carried out individually. However, in this study, with an array of antigen coating at different concentrations, the concentration-dependence therefore can be examined in a single experiment.

In order to test the specificity of the immunoassay, antigens from different bacteria were immobilized and assayed. The three different lysate antigens were *H. pylori* (30 μg/mL), *L. rhamnosus* (10 μg/mL) and *E. coli* (10 μg/mL), immobilized as indicated in Fig 9 (a). Immunoassay experiments were carried out under the conditions when the primary antibody solution contained only anti-*E. coli* antibody, or only anti- *H. pylori* antibody or both anti-*E. coli* and anti-*H. pylori* antibody. The secondary antibody solution contained a mixture of TRITC-conjugated anti-rabbit IgG and TRITC-conjugated anti-goat IgG in all runs. Images taken after the immunoassay are shown in Fig. 9 (b)-(d), while Fig. 9 (e)-(g) provide the corresponding fluorescence intensity profiles, obtained using MATLAB. Whenever a certain primary antibody was present, the corresponding antigen-coating site gave a detectable fluorescent signal. In addition, by comparing the profiles in Fig. 9 (e) and Fig. 9 (f) accordingly with Fig. 9 (g), it can be found that the fluorescent intensity is consistent, whether a certain primary antibody exists alone or in an antibody mixture. The site coated with *L.rhamnosus* lysate, used as a negative control, did not produce a visible signal in all runs. However, from Fig. 9 (c) and Fig. 9 (f), the *E. coli*-coating site gave a very weak signal when only anti-*H. pylori* antibody was present, indicating that a slight cross-reactivity existed between the *E. coli* antigen and polyclonal anti-*H. pylori* antibody. The good specificity of the immunoassay suggests potential applications in testing human serum, or other biological samples, for efficiently detecting multiple pathogen infections in a single assay. In the future, multiple testing channels can be easily integrated onto the same chip so that multiple samples can be tested simultaneously for the infection status.

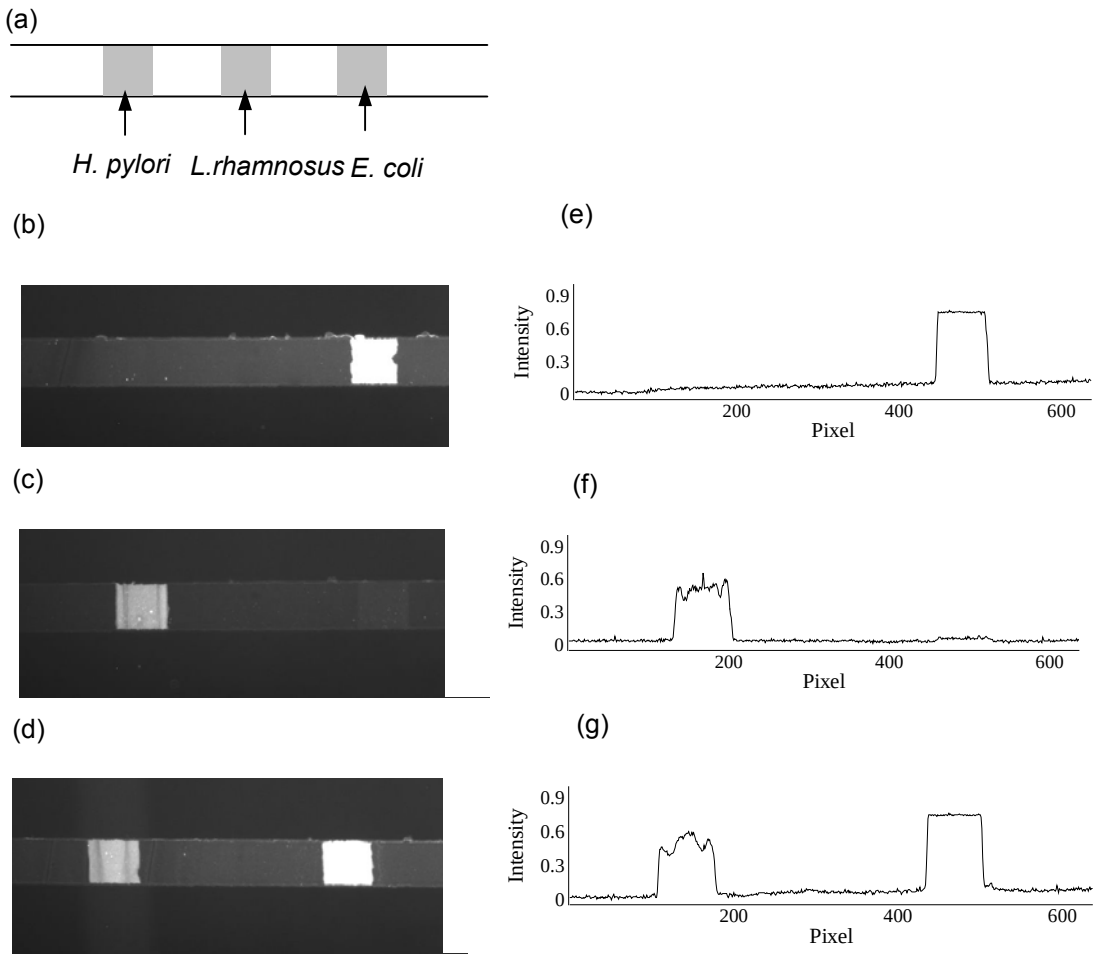

Figure 9: Specificity of the immunoassay. (a) The sites coated with different species of antigen (from left to right): *H. pylori* (30 μg/mL), *L.rhamnosus* (10 μg/mL), *E. coli* (10 μg/mL). (b)-(d) are fluorescence images, (e)-(g) are corresponding fluorescence intensity profiles. (b),(e) the primary antibody solution contained only anti-*E. coli*; (c),(f) the primary antibody solution contained only anti-*H. pylori*; (d),(g) the primary antibody solution contained a mixture of anti-*H. pylori* and anti-*E. coli*. The secondary antibody solution contained a mixture of TRITC-conjugated anti-rabbit IgG and TRITC-conjugated anti-goat IgG in all the cases.

5. Conclusions

Aimed at improving the automation and the detection multiplicity of miniaturized immunoassay, this study investigated an electrokinetically-controlled, multi-probing-coating immunoassay microchip. It is demonstrated that CFD is a very useful tool to find optimal parameter values for the design and the operation control of the on-chip immunoassay. The electrokinetically-controlled immunoassay microchip developed in this work performs all the sequential operations of the immunoassay in a FN automatically. The automatic operation, from dispensing of primary antibody to washing of secondary antibody, took 26 minutes. The total assay time, from antigen coating to signal detection, was one hour. These are significantly shorter than the assay time in conventional techniques. In addition, multiple immunoreactions can be assessed in one single experiment, with the existence of multiple antigen coating spots. The detection limit for *E. coli* lysate antigen was 3 μg/mL, comparable to that of the conventional dot-blot technique. When coated with different species of antigen, the immunoassay microchip can be used to screen a mixture of antibodies with good specificity.

Acknowledgements

This study was supported by a grant from Collaborative Health Research Project and Natural Sciences and Engineering Research Council of Canada (to D Li and PM Sherman), University of Toronto Open Fellowship (to YL Gao) and Canadian Institutes of Health Fellowship (to FYH Lin).

References

1. A. Ajdari, C.R. Physique. **5**, 539-546 (2004).
2. A. Bernard, B. Michel, and E. Delamarche, Anal. Chem. **73**, 8-12 (2001).
3. D. P. Bertsekas, *Constrained Optimization and Lagrange Multiplier Methods*. (Academic Press, New York, 1982).
4. E. Biddiss, D. Erickson, and D. Li, Anal. Chem. **76**, 3208-3213 (2004).
5. D.W. Chan, *Immunoassay Automatization.* (Academic Press, San Diego, CA, 1996).
6. N. Chiem, D. J. Harrison, Anal. Chem. **69**, 373-378 (1997).
7. E.B. Cummings, S. K. Griffiths, R.H. Nilson, P.H. Paul, Anal. Chem. **72**, 2526-2532 (2000).
8. E. Delamarche, A. Bernard, H. Schmid, A. Bietsch, B. Bichel and H. Biebuyck, J. Am. Chem. Soc. **120**, 500-508 (1998).
9. E. Delamarche, A. Bernard, H. Schmid, B. Michel, H. Biebuyck, Science. **276**, 779-781 (1997).
10. E.P. Diamandis and T.K.Christopoulos, *Immunoassay* (Academic Press, San Diego, CA, 1996) p. 1-3.
11. A. Dodge, K. Fluri, E. Verpoorte, and N.F.de Rooij, Anal. Chem. **73**, 3400-3409 (2001).
12. D. Erickson and D. Li, J. Phys. Chem. B. **107**, 12212-12220 (2003).
13. S. V. Ermakov, S. C Jacobson, and J. M. Ramsey, Anal. Chem. **70**, 4494-4504 (1998).
14. E Eteshola and D. Leckband, Sensors and Actuators B. **72**, 129-133 (2001).
15. G. Hu, Y.Gao, and D. Li, Microfluidics and Nanofluidics (in press).
16. X. Huang, M. J. Gordon, R. Zare, Anal. Chem. **60**, 1837-1838 (1988).
17. R.J. Hunter, *Zeta potential in colloid science, principals and applications* (Academic Press, New York, 1981).
18. X. Jiang, J. M. K. Ng, A. D. Stroock, S. K. W. Dertinger and G. M. Whitesides, J. Am. Chem. Soc. **125**, 5294-5295 (2003).
19. A.E. Jones, E. Grushka, J. Chromatogr. **466**, 219-225 (1989).
20. E. Kim, Y. Xia, and G.M. Whitesides, Nature. **376**, 581-584 (1995).
21. D. Li, *Electrokinetics in Microfluidics*. (Academic Press, New York, 2004).
22. F. Y. H. Lin, M. Sabri, D. Erickson, J. Alirezaie, D. Li and P. M. Sherman, Analyst. **129**, 823-828 (2004, A).
23. F. Y. H. Lin, P. M. Sherman and D. Li, Biomedical Microdevices. **6**, 125-130 (2004, B).
24. V. Linder, E. Verpoorte, N. F. de Rooij, H. Sigrist and W. Thormann, Electrophoresis. **23**, 740-749 (2002).
25. J. H. Masliyah, *Electrokinetic Transport Phenomena*. (AOSTRA, Edmonton, 1994).
26. N.A. Patankar and H.H. Hu, Anal. Chem. **70**, 1870-1881 (1998).
27. C.X. Qiu and J.D. Harrison, Electrophoresis. **22**, 3949-3958 (2001).
28. J.S. Rossier and H.H. Girault, Lab Chip. **1**, 153–157 (2001).
29. A. Rowe, S. B. Scruggs, M. J. Feldstein, J. P. Golden and F. S. Ligler, Anal. Chem. **71**, 433-439 (1999).
30. K. Sato, M. Tokeshi, H. Kimura and T. Kitamori, Anal. Chem. **73**, 1213-1218 (2001).
31. P. M. Sherman, E. Hassall, R. H. Hunt, C. A. Fallone, S. van Zanten and A. B. R. Thomson, Can. J. Gastroenterol. **13**, 553-559 (1999).

32. S. K. Sia, V. Linder, B. A.Parviz, A. Siegel and G. M. Whitesides, Angew. Chem. Int. Ed. **43**, 498–502 (2004).
33. H.A. Stone, A.D. Stroock, and A. Ajdari, Annual Review of Fluid Mechanics. **36**, 381-411 (2004).
34. A. Sze, D. Erickson, L. Ren and D. Li, J. Colloid Interf. Sci. **261**, 402-410 (2003).
35. P. I. Tarr, M.A. Neill, Clin. North. Am. **30**, 735-751 (2001).
36. N. Uemura, N. S. Okamoto, S. Yamamoto, N. Matsumura, S. Yamaguchi and M. Yamakido, K. Taniyama, N. Sasaki and R. J. Schlemper, N. Engl. J. Med. **345**, 784-789 (2001).
37. H.A. van der Vorst, SIAM J. Sci. Stat. Comput. **13**, 631-644 (1992).
38. J. Wang, A. Ibanez, M. P. Chatrathi and A. Escarpa, Anal. Chem. **73**, 5323-5327 (2001).
39. G. M. Whitesides and A. D.Stroock, Phys. Today. **54**, 42-49 (2001).
40. M. Wolf, D. Juncker, B. Michel, P. Hunziker, E. Delamarche, Biosens. Bioelectron. **19**, 1193-1202 (2004).
41. Y. Xia, G. M. Whitesides, Annu. Rev. Mater. Sci. **28**, 153–184 (1998).